Commun. Comput. Phys.
doi: 10.4208/cicp.260614.041214a

Vol. **18**, No. 3, pp. 558-576
September 2015

On the Finite Differences Used in Reacting Flow Simulations

Robert Prosser*

Department of Mechanical, Aerospace and Civil Engineering, University of Manchester, PO Box 88 Manchester M13 9PL, UK.

Received 26 June 2014; Accepted (in revised version) 4 December 2014

Abstract. There exist many spatial discretization schemes that are well able to provide accurate and stable approximations for isothermal turbulent flows. Comparatively little analysis has been made of the performance of these schemes in the presence of temperature gradients driven by combustion. In this paper, the effects of temperature gradients on numerical stability are explored. A surprising result is that temperature gradients in the flow have a tendency to impinge on *left half plane* (LHP) stability of the spatial discretization scheme. Reasons for this tendency are explored and two remedies are proposed: one based on the particular class of finite difference schemes, and one based on an alternative method of boundary condition specification.

AMS subject classifications: 76M20

Key words: Numerical methods, combustion, stability.

1 Introduction

1.1 Motivation

In a number of works on the Direct Numerical Simulation (DNS) of turbulent flows, observations have been made regarding the spurious generation of unphysical high frequency waves. For non-reacting flows, the origin of the spurious modes is thought to lie in the application of inexact time dependent boundary conditions leading to reflection [16]. A similar line of reasoning for reacting flows identifies leading order effects from viscous boundary conditions as providing additional channels for spurious modes [22]. The high order schemes typically used in DNS have low dissipation and thus the spurious modes may be long lasting, with an associated reduction in the fidelity of the simulation. Depending on the flow regime studied (i.e. low Reynolds number flow), the growth of the modes may be controlled to some extent by naturally dissipative

*Corresponding author. *Email address:* mcjssrp2@manchester.ac.uk (R. Prosser)

 ©2015 Global-Science Press

https://doi.org/10.4208/cicp.260614.041214a Published online by Cambridge University Press

processes (such as through viscosity or other transport phenomena) but, in general, best practise should not rely on physical processes to dissipate numerical artifacts. A number of high order filters have been designed explicitly with this problem in mind [13].

The widespread appearance of spurious modes in high fidelity DNS (whether caused by boundary conditions, under-resolution or some other agency) may be inferred by the prevalence of filtering in the literature, both in cold flow simulations (i.e. sponge layers both to absorb physical phenomena and—potentially—spurious artifacts [7]) and reacting flow studies, where filters are explicitly used during the simulation procedure [6, 11, 22, 27]. The role of the differencing schemes in the emergence, growth or propagation of these spurious modes is relatively unexplored in the context of computational combustion; the current work is motivated principally by this observation.

Fig. 1 shows a laminar flame solution for a single step chemical reaction mechanism with unit Lewis number, in which the thermochemical state of the gas is characterized by a *progress variable* (a normalized product mass fraction). The reaction rate has been adjusted to give a laminar flame speed of 30cm/s, a value typical of many hydrocarbon reactions. The mean flow is from left to right, counter to the flame's direction of propagation; by balancing the mean flow speed against the laminar flame speed, the flame is brought to rest relative to the computational domain. This specification gives a simulation Mach number of $\mathcal{O}\left(10^{-3}\right)$ based on the laminar flame speed. The simulation was performed using a mesh of 64 grid points. Profiles are given for temperature, density, velocity and pressure. The boundary conditions for this calculation use Navier-Stokes

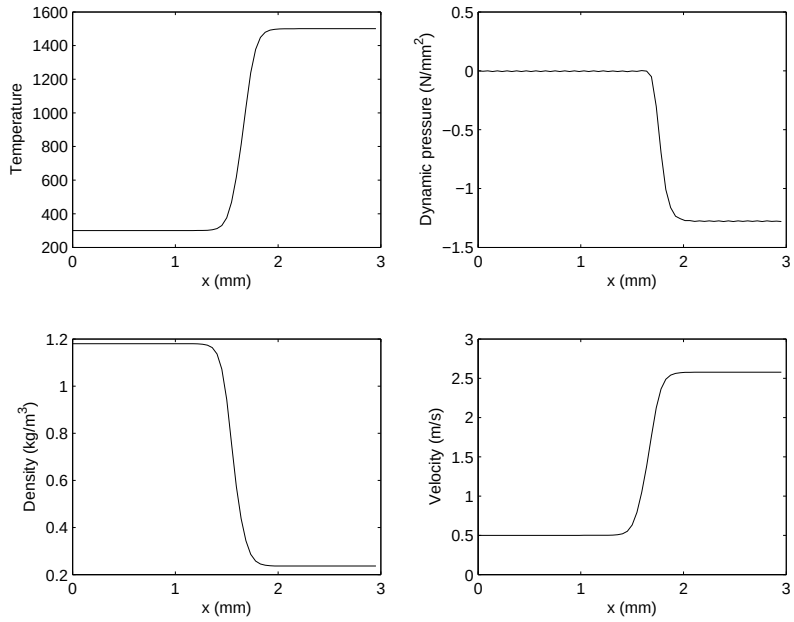


Figure 1: Example laminar flame solution for single step chemistry $R \to P$. Solution obtained using 4th order differences satisfying a *restricted norm* [21].

https://doi.org/10.4208/cicp.260614.041214a Published online by Cambridge University Press

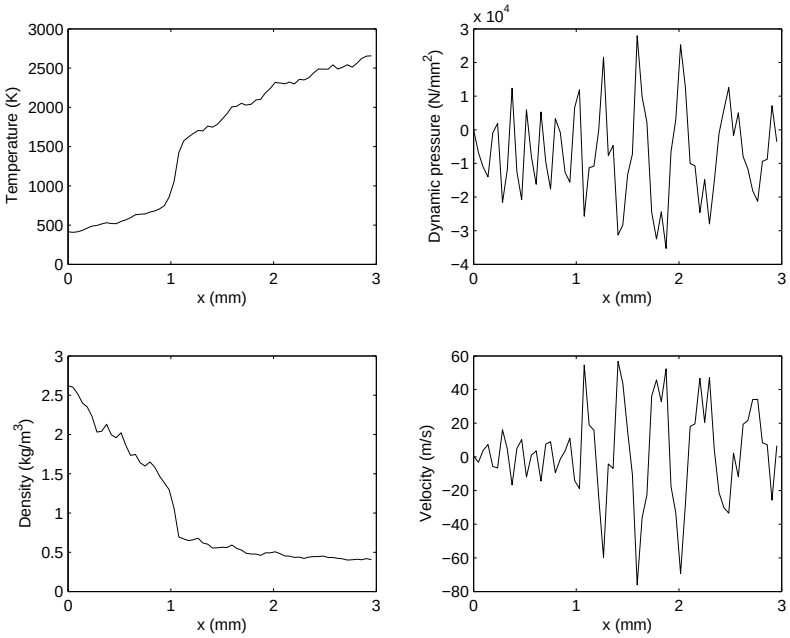


Figure 2: Example laminar flame solution for single step chemistry $R \to P$. Solution obtained using explicit 4th order differences derived via Taylor series.

Characteristic Boundary Conditions (NSCBC) [16] for the inviscid components, and zero gradients for temperature, species mass fraction and momentum transport terms.

Fig. 2 provides a second solution. This was obtained using the same flow configuration and boundary conditions as for Fig. 1; the differences in the solutions arise purely from the approximation used for the convective derivative. The profiles in Fig. 1 were calculated using an explicit 4th order centred difference scheme [21] with an associated *restricted norm* (discussed later), the solution in Fig. 2 was obtained using a 'standard' explicit 4th order scheme derived purely via Taylor series. The approximations are identical in the interior of the domain, and differ only their treatment of the near boundary nodes. The pressure in the latter case exhibits a growing oscillatory mode adjacent to the hot outflow boundary. The appearance of this mode appears to be insensitive to the choice of variables used to impose the boundary conditions, to the form of governing equations (conservative or primitive formulations) and to the choice of time stepping scheme (in both reported simulations, time integration was performed using a 3rd order Runge-Kutta method [26]). Alternative time integration methods have also been tested (but not reported here); these produce the same phenomena.

Fig. 3 gives results for an acoustic wave propagating through a chemically homogeneous, inviscid and quiescent fluid with a temperature gradient. The simulation was derived from the previous case by switching all transport and reaction effects off—which consequently renders the flow solenoidal [14,17,18]—and prescribing a temperature profile given by the laminar flame solution; from the thermal equation of state, $\rho(x) \propto T^{-1}(x)$,

https://doi.org/10.4208/cicp.260614.041214a Published online by Cambridge University Press

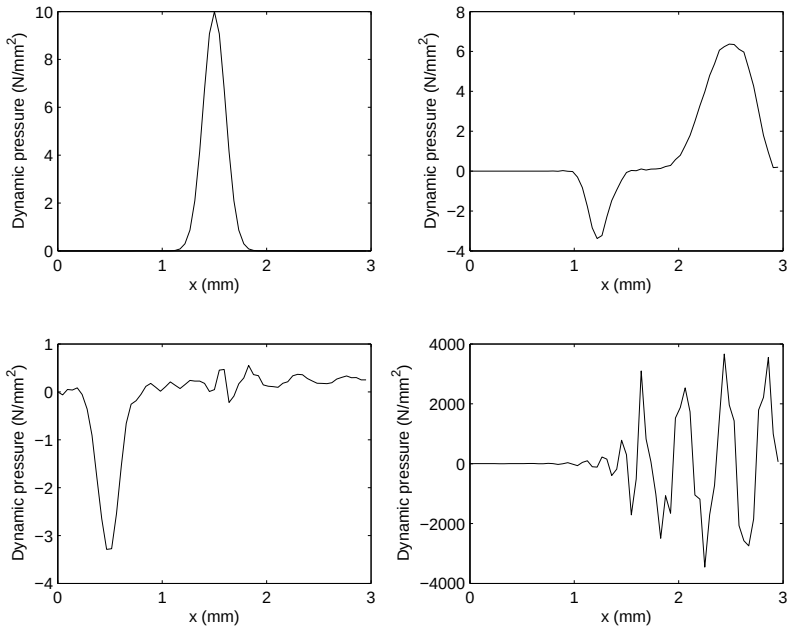


Figure 3: Acoustic wave propagating through the temperature profile given by the laminar flame solution. Results are taken at $t=0s$, $1.5\mu s$, $3.6\mu s$ and $36\mu s$, respectively.

and the initial (thermodynamic) pressure is thus assumed to be constant. These results are intended to convey the important observation that most of the difficulties encountered in Fig. 2 are related to the presence of temperature/density gradients in the evolving simulation coupled to the near boundary discretization schemes.

In this paper, the underlying reasons for the heat-release induced problems are explored, and strategies to mitigate the problem are presented. In Section 2, arguments are presented for a much simplified model problem which nevertheless exhibits the same oscillatory behaviour as a full reacting flow DNS. Section 3 reviews the techniques necessary to analyze the semi-discrete model problem, and also shows how heat release can have a dramatic effect on *Left Half Plane* (LHP) stability [13]. In Section 4, the *Simultaneous Approximation Term* approach (SAT) for boundary conditions is reviewed and applied to reacting flows for a number of differencing schemes. Calculations performed using the analysis are presented in Section 5 and the paper ends with conclusions and recommendations.

2 The model problem

With respect to numerical stability, much of the physics embodied in diffusion, dilatation and chemical reaction has only secondary importance. The numerical experiments exemplified by the acoustic wave in Fig. 3 indicate that the problems evident in full laminar

https://doi.org/10.4208/cicp.260614.041214a Published online by Cambridge University Press

flame calculations are strongly controlled by the flame induced variation in a (the speed of sound) acting on the *characteristic amplitudes* (defined in [16]). Since dilatation at low Mach number is driven by reaction and diffusion, it can be omitted by restricting attention to a chemically homogeneous source-free Euler system. For one dimensional systems, a decoupled set of equations for the Riemann invariants can be written as [1,16,23]:

$$\frac{\partial}{\partial t}(\mathbf{U})+\mathbf{S}^{-1}\mathbf{\Lambda}\mathbf{S}\frac{\partial}{\partial x}(\mathbf{U})=\mathbf{0}, \tag{2.1}$$

where $\mathbf{U}=\begin{pmatrix}\rho & u & P\end{pmatrix}^T$, $\mathbf{\Lambda}=diag(u-a,u,u+a)$, and $a=(\gamma RT)^{\frac{1}{2}}$. The effects of the flame on the Riemann invariants are modelled here through an essentially isobaric fluid with monotonic temperature distribution $T(x)$. The density is derived from the equation of the state for the gas: $\rho(x)\propto T^{-1}(x)$.

For a given set of initial conditions (given the suffix 0), consider small perturbations of the form $\rho=\rho_0(x,t)+\rho'$, $u=u_0(x,t)+u'$, and $p=p_0(x,t)+p'$. Introducing these perturbations into Eq. (2.1) and retaining only first order perturbations provides

$$\frac{\partial \mathbf{L}}{\partial t}+a_0(x)\mathbf{M}\frac{\partial \mathbf{L}}{\partial x}=0, \tag{2.2}$$

where $\mathbf{L}=\mathbf{S}\mathbf{U}$, $\mathbf{M}=diag\begin{pmatrix}M-1 & M & M+1\end{pmatrix}^T$ and M is the flow Mach number. In general, the right hand side of Eq. (2.2) contains a source vector arising as a result of density variations; this may be set to zero for the purposes of stability analysis [20].

The laminar flames motivating this analysis introduce a velocity scale into the simulations satisfying $u_0/a_0=M\ll 1$. Setting $M=0$ thus yields $u_0(x,t)=0$, $p_0(x,t)=const$, $\rho_0=\rho_0(x)$, $a_0=a_0(x)$ and the model problem driving the discussion in the rest of the paper:

$$\frac{\partial \phi}{\partial t}\pm a_0(x)\frac{\partial \phi}{\partial x}=0.$$

For definiteness, subsequent analysis will be based on the left-going advection equation which, in dimensionless variables, may be written as

$$\frac{\partial \phi}{\partial t}-a(x)\frac{\partial \phi}{\partial x}=0, \quad x\in[0,1), \tag{2.3}$$

$$\phi(1)=0, \tag{2.4}$$

with $1\le a(x)\le\sqrt{1+\tau}$. τ is a dimensionless temperature difference representing the heat released during combustion and is defined as $\tau=(T_\infty-T_0)/T_0$ [2].

3 Approximations to $\frac{d}{dx}$

3.1 The energy method

The importance of the approximation used to discretize d/dx in Eq. (2.3) has been extensively studied in the literature and, in the case of finite differences, stability properties

https://doi.org/10.4208/cicp.260614.041214a Published online by Cambridge University Press

are generally expressed via GKS analysis [10]. The algebraic complexity of this approach has led to a number of alternative formulations or interpretations of stability, such as that provided by Trefethen [24,25], or the *energy method*, which uses the definitions [21]

$$\begin{aligned}(u,v)&=\int_0^1 u^* v dx,\\ ||u||_2^2&=(u,u)\end{aligned} \tag{3.1}$$

to provide an energy bound for Eq. (2.3) [20]:

$$\frac{d}{dt}||\phi||_2^2=-a(0)\phi_0^2-\int_0^1\phi^2\frac{\partial a}{\partial x}dx\leq -a(0)\phi_0^2+A||\phi||_2^2, \tag{3.2}$$

where $A=\sup(-\partial a/\partial x)$, $\phi_0=\phi(0)$ and the boundary condition (Eq. (2.4)) has been applied. The behaviour of the norm in the continuous case provides the ideal limiting behaviour for the choice of semi-discretization and has been used as a guiding principle in the derivation of a number of finite difference schemes [3,12,21]. In isothermal flows $a(x)=const.$ and the energy of the solution satisfies.

$$\frac{d}{dt}||\phi||_2^2=-a\phi_0^2\leq 0. \tag{3.3}$$

3.2 The discrete problem – isothermal flows

An $(N+1)$ point semi-discretization of Eq. (2.3) onto a mesh of grid points $x_k=k\Delta h$, $0\leq k\leq N$, $h=N^{-1}$ yields

$$\frac{d\boldsymbol{\phi}}{dt}-\mathbf{A}\mathbf{Q}_B\boldsymbol{\phi}=0, \tag{3.4}$$

where $\boldsymbol{\phi}=(\phi(x_k))^T$, $\mathbf{A}=diag(\mathbf{a})$, $\mathbf{a}=(a(x_k))^T$ and $\mathbf{Q}_B$ embodies the finite difference scheme *and* the boundary condition (given by Eq. (2.4)). The method of implementation of the boundary condition has a strong impact on the behaviour of the overall scheme and will be re-visited later in the paper.

To provide a basis for comparison, the energy method is first discussed for the constant sound speed case, for which $\mathbf{A}=\mathbf{I}_{N+1}$. Discrete equivalents to the norm used in Eq. (3.1) are introduced as $(\mathbf{u},\mathbf{v})_H=\mathbf{u}^*\mathbf{H}\mathbf{v}$, $||\mathbf{u}||_H^2=(\mathbf{u},\mathbf{u})_H$, with $\mathbf{H}=\mathbf{H}^*>0$. Using these definitions, it is straightforward to show that the semi-discrete equivalent to Eq. (3.3) reads

$$\frac{d}{dt}||\boldsymbol{\phi}||_H^2=\boldsymbol{\phi}^*\left(\mathbf{H}\mathbf{Q}_B+(\mathbf{H}\mathbf{Q}_B)^*\right)\boldsymbol{\phi}. \tag{3.5}$$

To replicate the inequality appearing in Eq. (3.3), it is necessary that

$$\mathbf{H}\mathbf{Q}_B+(\mathbf{H}\mathbf{Q}_B)^*=-\mathbf{P}, \tag{3.6}$$

https://doi.org/10.4208/cicp.260614.041214a Published online by Cambridge University Press

where

$$\mathbf{P}=\begin{pmatrix}\mathbf{I}_1 & 0\\ 0 & 0\end{pmatrix}.$$

The bounding of the energy of the solution thus requires that the pair of matrices $(\mathbf{H},\mathbf{Q}_B)$ satisfy the Lyapunov equation (3.6); the condition $\mathbf{P}\geq 0$ is enforced by the application of the boundary condition $\phi(x_N)=0$. An equivalent expression of this boundedness is to describe the scheme as being Left Half Plane (LHP) stable, i.e. $\mathrm{Re}(\sigma(\mathbf{Q}_B))\leq 0$, where $\sigma(\mathbf{Q}_B)$ is the spectrum of $\mathbf{Q}_B$ [8]. This criterion is used extensively by Lele [13] in assessing the suitability of Pade schemes for high order accuracy flow simulations.

The energy method has been used to produce families of approximations and associated norm matrices in a number of papers (i.e. Kreiss and Scherer [12] and Carpenter et al. [3, 4]). In the latter works, the energy method is extended to incorporate families of compact finite differences defined by $\mathbf{Q}_B=\left(\mathbf{H}^{-1}\mathbf{Q}'\right)_B$, where $\mathbf{H}$ is band diagonal. For explicit differencing schemes, the energy method is used by Strand to provide approximations classed according to the norm with which they are equipped: *full, restricted* or *diagonal* norms [21]. In each of these latter cases, $\mathbf{H}$ is diagonal in the interior of the domain—the different classifications arise as a result of variations in the norm structure close to the boundaries.

It is worth noting that for any LHP stable finite difference scheme, there exists an associated norm matrix. The particular composition of $\mathbf{H}$ will generally depend also on the choice of boundary condition used to ensure $\mathbf{P}>0$. For most explicit difference schemes (i.e. those defined without recourse to energy methods), $\mathbf{H}$ is non-sparse; this observation has stability implications for flows with heat release, and is explored in the next section.

3.3 Problems arising from varying $a(x)$

LHP stability of $\mathbf{AQ}_B$ may be established via a generalized eigenvalue problem; in general, $\sigma(\mathbf{AQ}_B)$ is unrelated to $\sigma(\mathbf{Q}_B)$. An attempt to deduce the character of $\sigma(\mathbf{AQ}_B)$ might be made by trying to merge $\mathbf{A}$ and $\mathbf{H}$ in the energy method to form a new symmetric positive definite matrix. When applied to Eq. (3.4), such an approach leads to

$$\frac{d}{dt}\left(\boldsymbol{\phi}^*\widehat{\mathbf{H}}\boldsymbol{\phi}\right)=\boldsymbol{\phi}^*\left[\mathbf{A}^{-1},\mathbf{HQ}_B\right]\boldsymbol{\phi}-\boldsymbol{\phi}^*\mathbf{PA}^{-1}\boldsymbol{\phi}, \tag{3.7}$$

where the square brackets indicate the commutator. It can be readily established that $\widehat{\mathbf{H}}=\mathbf{A}^{-1}\mathbf{HA}^{-1}=\widehat{\mathbf{H}}^T>0$ and, since $\boldsymbol{\phi}^*\mathbf{PA}^{-1}\boldsymbol{\phi}\geq 0$, it follows that

$$\frac{d}{dt}||\phi||^2_{\widehat{H}}\leq\boldsymbol{\phi}^*\left(\left[\mathbf{A}^{-1},\mathbf{HQ}_B\right]\right)\boldsymbol{\phi}. \tag{3.8}$$

The condition $\left[\mathbf{A}^{-1},\mathbf{HQ}_B\right]\leq 0$ cannot be satisfied since the eigenvalues of a commutator sum to zero [15]. In terms of combustion, the heat release induced temperature gradients manifest themselves through $\mathbf{A}$ and adversely affect the stability of the discretisation.

https://doi.org/10.4208/cicp.260614.041214a Published online by Cambridge University Press

The analysis leading to Eq. (3.7) may be simplified if $\left[\mathbf{H},\mathbf{A}^{-1}\right]=0$, in which case it can be readily shown that

$$\frac{d}{dt}||\boldsymbol{\phi}||^2_{\widehat{H}}=-\boldsymbol{\phi}^*\mathbf{P}\boldsymbol{\phi}\leq 0, \tag{3.9}$$

where $\widehat{\mathbf{H}}=\mathbf{H}\mathbf{A}^{-1}=\widehat{\mathbf{H}}^T>0$. the requirement for $\mathbf{H}$ and $\mathbf{A}^{-1}$ to commute thus steers the choice of potential schemes.

3.4 Restricted and diagonal norm approximations

For explicit schemes, Strand has examined approximations whose associated norm matrix has the structure [21]

$$\mathbf{H}=\begin{pmatrix}\widetilde{\mathbf{H}} & 0\\ 0 & \mathbf{I}\end{pmatrix}. \tag{3.10}$$

$\widetilde{\mathbf{H}}$ is a symmetric positive definite matrix of size $n\times n$, $n\ll N$. From the preceding discussion, if $\widetilde{\mathbf{H}}$ is diagonal then $\left[\mathbf{A}^{-1},\mathbf{H}\right]=0$ and the differencing scheme may retain LHP stability for reacting flows: schemes with *diagonal norms* [21] should thus retain their stability properties in combustion simulations.

If $\widetilde{\mathbf{H}}$ is not diagonal, the resulting scheme can never be formally stable. Nevertheless, in practical calculations it may still be possible to achieve a well behaved simulation. From Eq. (3.10)

$$\left[\mathbf{A}^{-1},\mathbf{H}\right]=\begin{pmatrix}\mathbf{A}^{-1}\widetilde{\mathbf{H}}-\widetilde{\mathbf{H}}\mathbf{A}^{-1} & 0\\ 0 & 0\end{pmatrix}$$

and it follows that if the flame structure (temperature gradient) is sufficiently far from the boundary nodes, then locally, $\mathbf{A}$ is constant and $\left[\mathbf{A}^{-1},\mathbf{H}\right]\simeq 0$, $\mathbf{H}\mathbf{A}^{-1}\simeq\left(\mathbf{H}\mathbf{A}^{-1}\right)^T>0$ and Eq. (3.9) is approximately satisfied. In practical computations (where there is some small degree of dissipation arising from, say, transport or time integration approximations), the family of schemes with *restricted norms* may therefore also provide reasonable simulations (as demonstrated in Fig. 1).

4 The SAT method for heat-releasing flows

4.1 Isothermal flows

Establishing the properties of $\mathbf{A}\mathbf{Q}_B$ by re-calculating $\mathbf{H}$ is analogous to a problem in non-reactive flows that relates to the application of boundary conditions [5]. For the isothermal version of Eq. (3.4) (i.e. setting $\mathbf{A}=\mathbf{I}_{N+1}$), the usual method of applying boundary conditions is to calculate the spatial derivative *and then to set* $\phi'_N=0$. The model problem actually solved in practice is therefore

$$\frac{d\boldsymbol{\phi}}{dt}=\begin{pmatrix}\mathbf{I}_N & 0\\ 0 & 0\end{pmatrix}\mathbf{Q}\boldsymbol{\phi}=\mathbf{Q}''\boldsymbol{\phi}. \tag{4.1}$$

https://doi.org/10.4208/cicp.260614.041214a Published online by Cambridge University Press

While the pair $(\mathbf{H},\mathbf{Q})$ are usually designed without explicit reference to boundary conditions [3,4], the change from $\mathbf{Q}$ to $\mathbf{Q}''$ renders the original norm matrix irrelevant. In order to retain the structure both of $\mathbf{H}$ and $\mathbf{Q}$, the usual method of applying boundary conditions cannot be used. The parallels between $\mathbf{A}\mathbf{Q}_B$ and $\mathbf{Q}''$ are evident—in both cases, the original differencing scheme is modified by a premultiplying diagonal matrix.

For cold flows, an alternative method to impose the boundary condition may be obtained by retaining the complete differencing scheme and applying an additional *Simultaneous Approximation Term* (SAT) [5]. Applying SAT to Eq. (3.4) for an isothermal problem with boundary condition $\phi(1)=g(t)$ provides

$$\frac{d\boldsymbol{\phi}}{dt}=\widetilde{\mathbf{Q}}\phi+\varepsilon G_{NN}\mathbf{H}^{-1}\begin{pmatrix}0 & 0 & \cdots & g(t)\end{pmatrix}^T, \tag{4.2}$$

$$\widetilde{\mathbf{Q}}=\left(\mathbf{Q}-\varepsilon G_{NN}\mathbf{H}^{-1}\mathbf{B}\right), \tag{4.3}$$

$$\mathbf{B}=\begin{pmatrix}0 & 0\\ 0 & \mathbf{I}_1\end{pmatrix}, \tag{4.4}$$

$$\mathbf{G}=\left(\mathbf{H}\mathbf{Q}+(\mathbf{H}\mathbf{Q})^T\right). \tag{4.5}$$

For the finite difference schemes developed by Strand in [21] and by Carpenter et al. in [4,5], $\mathbf{G}$ has a special structure

$$\mathbf{G}=\begin{pmatrix}G_{00} & 0 & \cdots\\ 0 & 0 & 0\\ \vdots & 0 & G_{NN}\end{pmatrix}. \tag{4.6}$$

The energy norm for the *SAT* modified discretization yields (setting $g(t)=0$ for simplicity)

$$\boldsymbol{\phi}^T\mathbf{H}\frac{d\boldsymbol{\phi}}{dt}=\boldsymbol{\phi}^T\mathbf{H}\widetilde{\mathbf{Q}}\boldsymbol{\phi}=\boldsymbol{\phi}^T(\mathbf{H}\mathbf{Q}-\varepsilon G_{NN}\mathbf{B})\boldsymbol{\phi},$$

$$\frac{d}{dt}||\boldsymbol{\phi}||_H^2=G_{00}\phi_0^2+G_{NN}(1-2\varepsilon)\phi_N^2.$$

Hence, $\mathbf{H}\widetilde{\mathbf{Q}}<0$ and the energy of the system is bounded provided $G_{00}\leq 0$, $G_{NN}\geq 0$ (these conditions are met by candidate schemes satisfying integration by parts) and $\varepsilon\geq 1/2$.

4.2 Non-isothermal flows

For the case where temperature gradients within the solution are retained, the model equation is revised to incorporate SAT as

$$\frac{d\boldsymbol{\phi}}{dt}=\mathbf{A}\widetilde{\mathbf{Q}}\boldsymbol{\phi}, \tag{4.7}$$

https://doi.org/10.4208/cicp.260614.041214a Published online by Cambridge University Press

where $\widetilde{\mathbf{Q}}$ is defined in Eq. (4.3). Introducing $\boldsymbol{\psi}=\mathbf{A}^{-\frac{1}{2}}\boldsymbol{\phi}$, Eq. (4.7) can be re-written as

$$\boldsymbol{\psi}^T\mathbf{A}^{-\frac{1}{2}}\mathbf{H}\mathbf{A}^{-\frac{1}{2}}\frac{d\boldsymbol{\psi}}{dt}=\boldsymbol{\psi}^T\mathbf{A}^{-\frac{1}{2}}\mathbf{H}\widetilde{\mathbf{Q}}\mathbf{A}^{\frac{1}{2}}\boldsymbol{\psi}\leq 0.$$

The inequality arises from the observation that $\mathbf{A}^{-\frac{1}{2}}\mathbf{H}\widetilde{\mathbf{Q}}\mathbf{A}^{\frac{1}{2}}$ is a similarity transform of $\mathbf{H}\widetilde{\mathbf{Q}}\leq 0$. Since $\left|\left|\mathbf{A}^{-\frac{1}{2}}\boldsymbol{\psi}\right|\right|_H^2\to 0$ and $\left|\left|\mathbf{A}^{-\frac{1}{2}}\right|\right|_H$ is constant, $||\boldsymbol{\phi}||_H^2\to 0$ and the SAT approach thus remains LHP stable for flows with temperature gradients.

4.3 SAT and other compact schemes

For the general class of compact finite difference schemes described by Lele [13], **G** does not have the simple structure given by Eq. (4.6). Given the ubiquity of compact schemes in reacting flow DNS, it is worthwhile examining whether the SAT approach may be appropriately extended to include these approximations.

For reasons to be made clear shortly, attention is restricted to the fourth order tridiagonal compact scheme with third order boundary closure (and referred to hereafter as the 4–3 compact scheme) [13];

$$\mathbf{H}=\begin{pmatrix} 1 & \frac{1}{4} & 0 & \cdots \\ \frac{1}{4} & 1 & \frac{1}{4} & \\ 0 & \ddots & \ddots & \ddots \\ \vdots & & \ddots & \ddots \end{pmatrix},\quad \mathbf{Q}'=\begin{pmatrix} -\frac{23}{12} & \frac{23}{8} & -\frac{5}{4} & \frac{7}{24} & 0 & \cdots \\ -\frac{3}{4} & 0 & \frac{3}{4} & & & \\ 0 & -\frac{3}{4} & 0 & \frac{3}{4} & & \\ \vdots & & \ddots & \ddots & \ddots & \end{pmatrix}. \tag{4.8}$$

Note that $\mathbf{Q}=\mathbf{H}^{-1}\mathbf{Q}'$ in the notation of this paper, and that Eq. (4.5) becomes $\mathbf{G}=\mathbf{Q}'+(\mathbf{Q}')^T$.

To apply the SAT scheme, assume that **Q** will be modified only through its treatment of ϕ_N and split **G** according to

$$\mathbf{G}=\left(\mathbf{G}_0+\mathbf{G}_0^T\right)+\left(\mathbf{G}_N+\mathbf{G}_N^T\right),$$

where

$$\mathbf{G}_0=\left(\widetilde{G}^{(0)}|0|\cdots|0\right),$$
$$\mathbf{G}_N=\left(0|0|\cdots|\widetilde{G}^{(N)}\right).$$

$\widetilde{G}^{(0)}\left(\widetilde{G}^{(N)}\right)$ is the $0^{th}\left(N^{th}\right)$ column vector of the matrix defined by Eq. (4.5) with a modification to the first(last) component

$$\widetilde{G}_k^{(0)}=\begin{cases}\frac{1}{2}G_k^{(0)}, & k=0,\\ G_k^{(0)}, & 1\leq k\leq N,\end{cases}$$
$$\widetilde{G}_k^{(N)}=\begin{cases}G_k^{(N)}, & 0\leq k\leq N-1,\\ \frac{1}{2}G_k^{(N)}, & k=N.\end{cases}$$

https://doi.org/10.4208/cicp.260614.041214a Published online by Cambridge University Press

Introducing the boundary modified operator and setting $\varepsilon=1$ for simplicity

$$\widetilde{\mathbf{Q}}=\mathbf{Q}-\varepsilon\mathbf{H}^{-1}\mathbf{G}_N=\mathbf{H}^{-1}\left(\mathbf{Q}'-\mathbf{G}_N\right), \tag{4.9}$$

it is straightforward to demonstrate that with this construction

$$\begin{aligned}&\frac{d\boldsymbol{\phi}}{dt}=\widetilde{\mathbf{Q}}\boldsymbol{\phi}, \\ &\frac{d}{dt}||\boldsymbol{\phi}||_H^2=\boldsymbol{\phi}^T\left(\mathbf{Q}'+\left(\mathbf{Q}'\right)^T\right)\boldsymbol{\phi}-\boldsymbol{\phi}^T\left(\mathbf{G}_N+\mathbf{G}_N^T\right)\boldsymbol{\phi}=\boldsymbol{\phi}^T\left(\mathbf{G}_0+\mathbf{G}_0^T\right)\boldsymbol{\phi}.\end{aligned} \tag{4.10}$$

Boundedness immediately follows if $\left(\mathbf{G}_0+\mathbf{G}_0^T\right)\leq 0$ for the set of eigenvectors allowed by $\widetilde{\mathbf{Q}}$.

Writing the solution to Eq. (4.10) in the form $\phi=\sum_m\beta_m(t)\mathbf{v}_m(\mathbf{x})$, where $\mathbf{v}_m(\mathbf{x})$ are the right eigenvectors of $\widetilde{\mathbf{Q}}$, and introducing the matrix

$$\mathbf{R}=(\beta_0(t)\mathbf{v}_0|\beta_1(t)\mathbf{v}_1|\beta_2(t)\mathbf{v}_2|\cdots|\beta_N(t)\mathbf{v}_N),$$

Eq. (4.10) provides

$$\frac{d}{dt}(\mathbf{R}^*\mathbf{H}\mathbf{R})=\mathbf{R}^*\left(\mathbf{G}_0+\mathbf{G}_0^T\right)\mathbf{R} \tag{4.11}$$

in which $Tr(\mathbf{R}^*\mathbf{H}\mathbf{R})=\sum_m|\beta_m(t)|^2||\mathbf{v}_m||_H^2=||\phi||_H^2$. Introducing $\det(\mathbf{R}^*\mathbf{H}\mathbf{R})\geq 0$ then, if the energy of the solution decreases it follows that $|\beta_m(t)|^2\to 0$ and hence $\det(\mathbf{R}^*\mathbf{H}\mathbf{R})\to 0$. Re-writing Eq. (4.11) to exploit this observation yields

$$\begin{aligned}\frac{1}{\det(\mathbf{R}^*\mathbf{H}\mathbf{R})}\frac{d}{dt}(\det(\mathbf{R}^*\mathbf{H}\mathbf{R}))&=Tr\left((\mathbf{R}^*\mathbf{H}\mathbf{R})^{-1}\frac{d}{dt}(\mathbf{R}^*\mathbf{H}\mathbf{R})\right)\\&=Tr\left(\mathbf{H}^{-1}\left(\mathbf{G}_0+\mathbf{G}_0^T\right)\right).\end{aligned}$$

$||\phi||_H^2\to 0$ if $Tr\left(\mathbf{H}^{-1}\left(\mathbf{G}_0+\mathbf{G}_0^T\right)\right)\leq 0$. The practical calculation of the trace is simplified by writing $\mathbf{H}^{-1}=\boldsymbol{\eta}\boldsymbol{\Lambda}^{-1}\boldsymbol{\eta}^*$, where $\boldsymbol{\Lambda}$ is the diagonal matrix of eigenvalues of $\mathbf{H}$. Although analytic expressions exist for the eigenmodes of $\mathbf{H}$ in Eq. (4.8) directly [19], the simplest demonstration of boundedness can be made by replacing $\mathbf{H}$ with the *asymptotically similar* circulant matrix $\mathbf{H}_c$ [9]

$$\mathbf{H}_c=\begin{pmatrix}1&\frac{1}{4}&0&\cdots&\frac{1}{4}\\ \frac{1}{4}&1&&&0\\ 0&&\ddots&&0\\ \vdots&&&\ddots&\vdots\\ \frac{1}{4}&0&&\frac{1}{4}&1\end{pmatrix}.$$

It is for the sake of this substitution that attention is restricted to the 4–3 compact scheme given by Eq. (4.8).

https://doi.org/10.4208/cicp.260614.041214a Published online by Cambridge University Press

4.3.1 Calculating the elements of the trace

The eigenmodes for $\mathbf{H}_c \in \Re^{(N+1)\times(N+1)}$ are

$$\lambda_k = 1+\frac{1}{2}\cos\left(\frac{2\pi k}{N+1}\right), \tag{4.12}$$
$$\mathbf{v}_k = (N+1)^{-\frac{1}{2}}\left(1,\exp\left(-\frac{2\pi ik}{N+1}\right),\exp\left(-\frac{4\pi ik}{N+1}\right),\cdots,\exp\left(-\frac{2\pi ikN}{N+1}\right)\right)^T,$$

where $(N+1)^{-\frac{1}{2}}$ is used to normalize the eigenvectors.

Using this decomposition, the upper left elements of the matrix $\mathbf{H}_c^{-1}$ can be shown to comprise

$$\mathbf{H}_c^{-1} = (N+1)^{-1}\begin{pmatrix} \sum_k \lambda_k^{-1} & \sum_k \lambda_k^{-1}\exp\left(\frac{2\pi i}{N+1}k\right) & \sum_k \lambda_k^{-1}\exp\left(\frac{2\pi i}{N+1}(2k)\right) & \cdots \\ \sum_k \lambda_k^{-1}\exp\left(-\frac{2\pi i}{N+1}k\right) & \ddots & & \\ \sum_k \lambda_k^{-1}\exp\left(-\frac{2\pi i}{N+1}(2k)\right) & & \ddots & \\ \vdots & & & \ddots \end{pmatrix},$$

with the remaining elements not required for this discussion. The expressions for the trace components of the compact 4–3 scheme may now be explicitly calculated as

$$(N+1)\left(\mathbf{H}_c^{-1}\left(\mathbf{G}_0+\mathbf{G}_0^T\right)\right)_{mm} = \begin{cases} \sum_{n=0}^{3} G_{nm}\left(\sum_k \lambda_k^{-1}\exp\left(\frac{2\pi i}{N+1}(nk)\right)\right), & m=0, \\ G_{0m}\sum_k \lambda_k^{-1}\exp\left(-\frac{2\pi i}{N+1}(mk)\right), & 1\le m\le 3, \\ 0, & m>3. \end{cases} \tag{4.13}$$

$\left(\mathbf{H}^{-1}\left(\mathbf{G}_0+\mathbf{G}_0^T\right)\right)_{00} < 0$ may be established directly by noting that $G_{00}<0$ and $|G_{00}| > \sum_{k=1}^{3}|G_{k0}|$.

The sign of $\left(\mathbf{H}^{-1}\left(\mathbf{G}_0+\mathbf{G}_0^T\right)\right)_{11}$ is obtained by first using Eq. (4.12) to re-write the second equation of Eq. (4.13) as

$$G_{01}\sum_k \lambda_k^{-1}\exp\left(-\frac{2\pi i}{N+1}k\right) = G_{01}\sum_k\left(1+\frac{1}{2}\cos\left(\frac{2\pi k}{N+1}\right)\right)^{-1}\exp\left(-\frac{2\pi i}{N+1}k\right).$$

As $\mathbf{H}_c^{-1}\left(\mathbf{G}_0+\mathbf{G}_0^T\right)$ is strictly real, the imaginary component must vanish and may be disregarded from further analysis.

The remaining terms can be approximated using the observation

$$\int_0^{2\pi}\frac{\cos(x)}{1+\frac{1}{2}\cos(x)}dx \simeq \left(\frac{2\pi}{N+1}\right)\sum_{k=0}^{N}\frac{\cos\left(\frac{2\pi}{N+1}k\right)}{1+\frac{1}{2}\cos\left(\frac{2\pi k}{N+1}\right)}$$

https://doi.org/10.4208/cicp.260614.041214a Published online by Cambridge University Press

and—providing the resolution is sufficiently high—the (easier to evaluate) integral may be used to replace the summation. This then provides

$$G_{01}\sum_k \lambda_k^{-1}\exp\left(-\frac{2\pi i}{N+1}k\right) \simeq G_{01}\left(\frac{N+1}{2\pi}\right)\int_0^{2\pi}\frac{\cos(x)}{1+\frac{1}{2}\cos(x)}dx$$
$$= G_{01}\frac{N+1}{2}\left(4-\frac{8}{\sqrt{3}}\right)\leq 0.$$

A similar approach for the remaining terms yields

$$G_{02}\sum_k \lambda_k^{-1}\exp\left(-\frac{2\pi i}{N+1}(2k)\right) \simeq G_{02}\frac{N+1}{2}\left(\frac{28}{\sqrt{3}}-16\right)\leq 0,$$
$$G_{03}\sum_k \lambda_k^{-1}\exp\left(-\frac{2\pi i}{N+1}(3k)\right) \simeq G_{03}\frac{N+1}{2}\left(60-\frac{104}{\sqrt{3}}\right)\leq 0.$$

It follows then that $\frac{d}{dt}(\det(\mathbf{R}^*\mathbf{HR}))\leq 0$ and the SAT approach applied to the compact 4–3 scheme also satisfies $\mathbf{HQ}\leq 0$. Applying the same reasoning as used in Section 4.2, the compact 4–3 scheme may be used with SAT for reacting flows.

The stability of the SAT approach has been verified for the 4–3 compact scheme by explicitly analysing the eigenvalues of the resulting approximation. At the same time, spectra have been calculated numerically for uniform 4th order and compact 6th order schemes from the same family of approximations (not shown here). These too have been observed to be stable with the inclusion of the SAT boundary modification. There is as yet no proof of why this should be so, since the boundary constructions of these latter schemes do not lend themselves to approximation via circulant matrices. This more general case is currently being further pursued.

5 Results

Test calculations have been undertaken to verify the stability properties described above. Each calculation is associated with a particular semi-discretisation of Eq. (3.4) and method of boundary condition application. The calculations are defined on the interval $x\in[0,1)$, discretised using 65 grid points. The dimensionless propagation speed is given by

$$\mathbf{A} = diag(a(x_i)),$$
$$a(x_i) = \left(1+\frac{\tau}{2}(1+\tanh(20(x_i-0.5)))\right)^{\frac{1}{2}},$$
$$\tau = 4,$$

and the initial conditions ϕ_0 are given by

$$\phi_0(x_i) = \exp\left(-\left(30\left(x_i-\frac{3}{4}\right)\right)^2\right).$$

https://doi.org/10.4208/cicp.260614.041214a Published online by Cambridge University Press

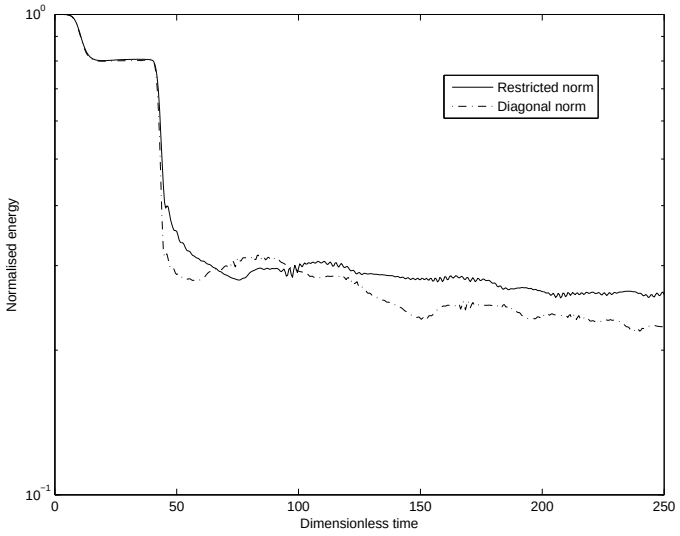


Figure 4: Normalised energy history for restricted norm and diagonal norm approximations to d/dx.

The analytical solution to this problem is

$$\boldsymbol{\phi}(t) = \exp(\mathbf{AQ}t)\boldsymbol{\phi}_0.$$

Time histories of the normalized energy $||\boldsymbol{\phi}(t)||_H^2 / ||\boldsymbol{\phi}_0||_H^2$ are plotted in Figs. 4 and 6. The distinctive double reduction in each solution's energy is caused by two processes: in the first process, the leading edge of the wave slows down and is caught by the trailing edge as the wave propagates through the temperature gradient. The amplitude of the wave remains constant as it slows and this produces an associated reduction in $||\boldsymbol{\phi}(t)||_H^2$. The constancy of the wave's amplitude during this process can be verified analytically by introducing the coordinate change $\xi = \int^x a^{-1}(x')dx'$ into Eq. (2.3) and observing that the solution obeys $\phi(\xi - t) = \phi_0$. The second energy reduction is associated with the wave leaving the domain.

Fig. 4 provides the histories for the normalized energies associated with the diagonal and restricted norm discretisations. In each case, the solution evolves to a point where $||\boldsymbol{\phi}(t)||_2 / ||\boldsymbol{\phi}_0||_2 \approx 0.2$ at which time the energy in the domain effectively reaches a minimum. The minimum corresponds to the energy associated with the eigenmodes satisfying $\mathrm{Re}(\lambda_k) \approx 0$ (the spectra for the two schemes are given in Fig. 5); these modes have extremely slow decay rates.

Fig. 6 depicts the normalized energy decay for the 4–3 compact scheme and for a 6th order scheme with 4th order boundaries (denoted 6–4–4 to reflect the internal, intermediate and boundary accuracies, respectively) [13]. Boundary conditions are imposed using the SAT approach. Unlike the restricted and diagonal norm cases, the energy here continues to decay towards zero. The rate at which the energy approaches zero has been found numerically to depend only very weakly on the choice of ε in Eq. (4.9); in the absence of

https://doi.org/10.4208/cicp.260614.041214a Published online by Cambridge University Press

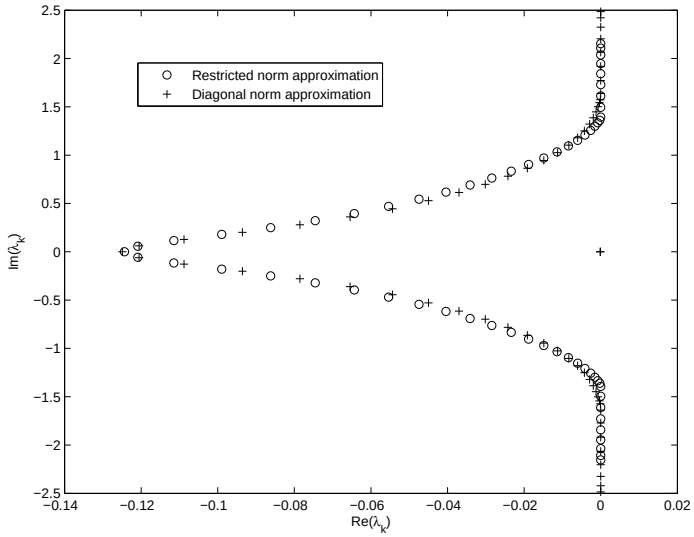


Figure 5: $\sigma(\mathbf{Q})$ for restricted and diagonal norm approximations to d/dx.

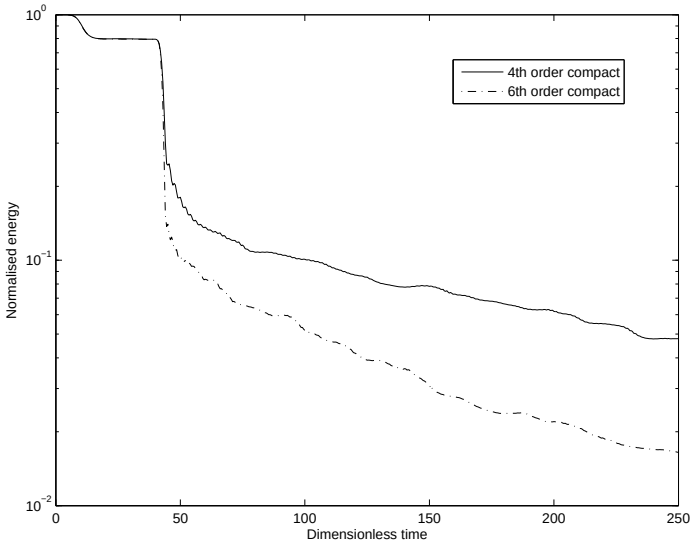


Figure 6: Normalised energy history for 4^{th} order compact and 6^{th} order compact approximations to d/dx, with boundary conditions implemented via SAT.

any compelling evidence, there appears no reason to select any value other than $\varepsilon = 1$. Fig. 7 shows the spectrum of the compact operators with the SAT boundary condition. Since there are relatively fewer eigenvalues very close to the imaginary axis there are correspondingly fewer long lasting energy carrying eigenmodes in the discretization. This translates into the increased rate of decay of the energy seen in Fig. 6.

https://doi.org/10.4208/cicp.260614.041214a Published online by Cambridge University Press

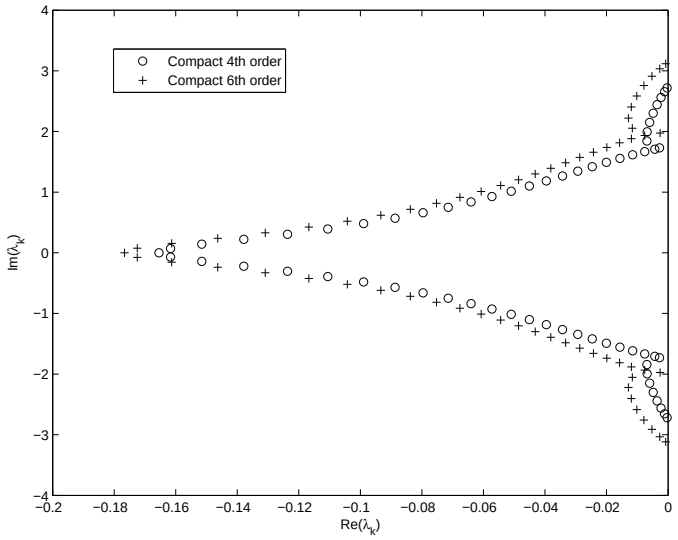


Figure 7: $\sigma(\mathbf{Q})$ for SAT modified compact 4^{th} order and compact 6^{th} order approximations to d/dx.

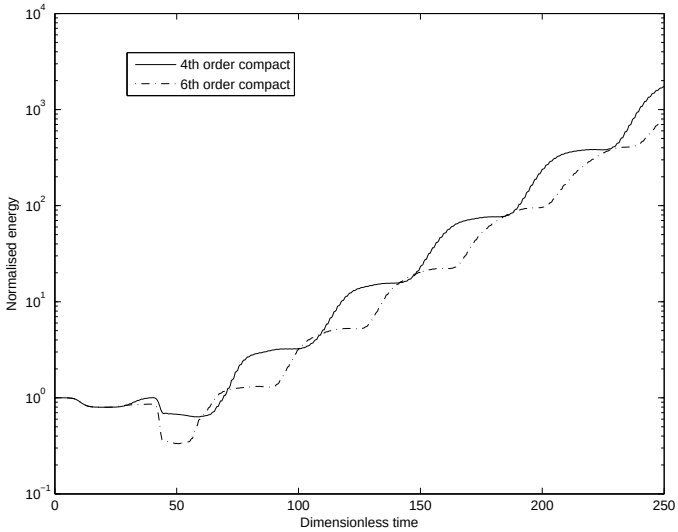


Figure 8: Normalised energy history for 4^{th} order compact and 6^{th} order compact approximations to d/dx, with 'standard' boundary condition implementation.

For completeness, Fig. 8 depicts the normalized energy behaviour for the 4–3 and 6–4–4 compact finite difference schemes using a simple boundary condition application (i.e. calculate the derivative for all grid points and then set $\phi'(x_N)=0$). In both cases, the energy grows rapidly and produces an instability similar to that shown in Fig. 3.

https://doi.org/10.4208/cicp.260614.041214a Published online by Cambridge University Press

6 Conclusions

The prevailing view in the reacting flow community appears to be that local operators produce local effects; the coupling hidden in (often dense) norm matrices and its role in the integration of the governing equations has been largely bypassed. In this paper, numerical instability arising from heat release has been investigated. Spatial discretization schemes that provide stable approximations for cold flows cannot be assumed to be stable for flows with heat release. The destabilizing effect is separate to the non-linear processes of combustion and convection, and grows from purely numerical origins which, in turn, are driven by the application of boundary conditions. The importance of the norm matrix associated to the differential operator is underscored; the application of boundary conditions and/or the presence of a heat release layer can ruin the desirable properties of a numerical scheme (i.e. its integration by parts property). The norm matrices can either be designed into a scheme, or calculated after the fact via the Lyapunov equation. The latter approach is used for the explicit finite differences traditionally developed from a simple Taylor series expansion. To find the norm matrix in that case, the Lyapunov equation must have the boundary condition already built into the operator (since otherwise, the equation would not have a negative definite solution); the resulting solution is both non-sparse *and* dependent on the position of the heat release layer. The heat release tends to cause the spectrum of points to migrate into the right half plane and instability ensues.

Schemes which remain useable in the presence of heat release have been identified.

- The classes of operators with *diagonal* and *restricted* norms [21] can be used with a straightforward boundary condition implementation. The latter class of approximations come with the caveat that the heat release layer must not approach the boundary close enough to corrupt the locally non-sparse norm matrix there.
- The families of tri-diagonal schemes developed by Carpenter et al. [3–5] have been shown to be stable for heat releasing flows, provided the boundary conditions are applied via a *Simultaneous Approximation Term* (SAT) approach. The presence of heat release does not corrupt the integration by parts property explicitly retained by the SAT method.
- An application of the SAT method to a 4–3 compact finite difference scheme has produced a stable formulation for non-isothermal problems. A demonstration of why this approach is stable has been provided. The 'standard' 6–4–4 compact finite difference [13] has also been found numerically to be stable using a SAT-type approach. There is as no yet a proof as to why (or indeed if) this should be so; this is part of ongoing work.

Acknowledgments

The author gratefully acknowledges the referees, Prof. R.S. Cant and Prof. S.V. Utyuzhnikov for their helpful comments regarding draft versions of this manuscript.

https://doi.org/10.4208/cicp.260614.041214a Published online by Cambridge University Press

References

[1] M. Baum, T.J. Poinsot, and D. Thévenin. Accurate boundary conditions for multicomponent reactive flows. J. Comput. Phys., 116:247–261, 1994.

[2] R.S. Cant and E. Mastorakos. An Introduction to Turbulent Reacting Flows. Imperial College Press, 2008.

[3] M.H. Carpenter, D. Gottlieb, and S. Abarbanel. Stable and accurate boundary treatments for compact, high-order finite-difference schemes. Appl. Numer. Math., 12:55–87, 1993.

[4] M.H. Carpenter, D. Gottlieb, and S. Abarbanel. The stability of numerical boundary treatments for compact high-order finite-difference schemes. J. Comput. Phys., 108:272–295, 1993.

[5] M.H. Carpenter, D. Gottlieb, and S. Abarbanel. Time-stable boundary conditions for finite-difference schemes solving hyperbolic systems: Methodology and application to high-order compact schemes. J. Comput. Phys., 111:220–236, 1994.

[6] J.H. Chen, A. Choudhary, B. de Supinsky, M. DeVries, E.R. Hawkes, S. Klasky, W.K. Liao, K.L. Ma, J. Mellor-Crummey, N. Podhorszki, R. Sankaran, S. Shende, and C.S. Yoo. Terascale direct numerical simulations of turbulent combustion using S3D. Comput. Sci. Discov., 2:2–32, 2009.

[7] T. Colonius, S.K. Lele, and P. Moin. Sound generation in a mixing layer. J. Fluid Mech., 330:375–409, 1997.

[8] I.S. Gradshteyn and I.M. Ryzhik. Table of Integrals, Series and Products. Academic Press, 6th edition, 2000.

[9] R.M. Gray. Toeplitz and circulant matrices: A review. Foundations and Trends in Communication and Information Theory, 2:155–239, 2006.

[10] B. Gustafsson, H.-O. Kreiss, and A. Sundstr¨m. Stability theory of difference approximations for mixed initial boundary value problems. II. Math. Comput., 26:649–686, 1972.

[11] C.A. Kennedy and M.H. Carpenter. Several new methods for compressible shear-layer simulations. Appl. Numer. Math., 14:397–433, 1994.

[12] H.O. Kreiss and G. Scherer. Mathematical Aspects of Finite Elements in Partial Differential Equations. Academic Press, 1977.

[13] S.K. Lele. Compact finite difference schemes with spectral-like resolution. J. Comput. Phys., 103:16–42, 1992.

[14] A. Majda and J. Sethian. The derivation and numerical solution of the equations for zero mach number combustion. Combust. Sci. and Tech., 42:185–205, 1985.

[15] E.A. Martins and F.C. Silva. Eigenvalues of matrix commutators. Linear and Multilinear Algebra, 39:375–389, 1995.

[16] T.J. Poinsot and S.K. Lele. Boundary conditions for direct simulations of compressible viscous flows. J. Comput. Phys., 101:104–129, 1992.

[17] R. Prosser. Towards improved boundary conditions for the DNS and LES of turbulent subsonic flows. J. Comput. Phys., 222:469–474, 2007.

[18] R. Prosser. Improved boundary conditions for the DNS of reacting subsonic flows. Flow Turbul. Combust., 87:351–376, 2011.

[19] S.S. Reddi. Eigenvector properties of Toeplitz matrices and their application to spectral analysis of time series. Signal Process., 7:45–56, 1984.

[20] V.S. Ryaben'kii and S.V. Tsynkov, editors. A Theoretical Introduction to Numerical Analysis. Chapman & Hall/CRC, 2007.

[21] B. Strand. Summation by parts for finite difference approximations for d/dx. J. Comput. Phys., 110:47–67, 1994.

https://doi.org/10.4208/cicp.260614.041214a Published online by Cambridge University Press

[22] J.C. Sutherland and C.A. Kennedy. Improved boundary conditions for viscous, reacting, compressible flows. J. Comput. Phys., 191:502–24, 2003.
[23] K.W. Thompson. Time dependent boundary conditions for hyperbolic systems. J. Comput. Phys., 68:1–24, 1987.
[24] L.N. Trefethen. Group velocity in finite difference schemes. SIAM Review, 24:113–136, 1982.
[25] L.N. Trefethen. Group velocity interpretation of the stability theory of Gustaffson, Kreiss and Sundström. J. Comput. Phys., 49:199–217, 1983.
[26] A.A. Wray. Minimal Storage Time-Advancement Schemes for Spectral Methods. NASA Ames Research Center, 1990.
[27] C.S. Yoo, Y. Wang, A. Trouvé, and H.G. Im. Characteristic boundary conditions for direct simulations of turbulent counterflow flames. Combust. Theory Modelling, 9:617–646, 2005.

https://doi.org/10.4208/cicp.260614.041214a Published online by Cambridge University Press